Quantum-driven phase transition in ice described via an efficient Langevin approach

Yael Bronstein,[1,2] Philippe Depondt,[1,2] Fabio Finocchi,[1,2] and Antonino Marco Saitta[3,4]

[1]*Sorbonne Universités, UPMC Université Paris 6, UMR 7588, INSP, F-75005 Paris, France*

[2]*CNRS, UMR 7588, INSP, F-75005 Paris, France*

[3]*Sorbonne Universités, UPMC Université Paris 6, UMR 7590, IMPMC, F-75005 Paris, France*

[4]*CNRS, UMR 7590, IMPMC, F-75005 Paris, France*

The phase transition from ice VII to ice X under extreme pressures is an example where quantum proton delocalization coexists with classical thermal fluctuations. We investigate this transition, including quantum effects on the nuclear motion through adapted Langevin dynamics. This approach, which allows us to follow the semiclassical trajectories of protons, provides excellent agreement with experimental vibrational spectra indicating a transition pressure of about 65 GPa. Furthermore, we map the full dynamical problem onto a pressure-dependent, one-dimensional mean-field potential for the proton. By solving exactly the corresponding Schrödinger equation, we disentangle tunneling and quantum delocalization from classical thermal effects and identify the transition through the topological changes of the proton ground state and its susceptibility. The process is dominated by quantum effects even at ambient temperature and can be considered to be a paradigmatic case of a quantum-driven phase transition.

I. INTRODUCTION

As the thermal wavelength of a proton is far from negligible with respect to interatomic distances, its quantum nature is central to the static and dynamical properties of hydrogen-based systems. Nuclear quantum effects (NQE) are pivotal in various phenomena such as proton tunneling, isotopic fractionation, and phase transitions in hydrogen-bonded systems [1]. They may also play a role in technologically relevant problems such as hydrogen storage and influence the performance of batteries and fuel cells [2]. However, the systematic understanding of NQE is often lacking in those systems, partly because quantum effects on nuclear dynamics can be blurred by the structural complexity and other competing phenomena [2–4].

We revisit here ice under high pressure as a prototypical system for studying NQE from a quantitative perspective. Phase VII of ice has a cubic structure, with disordered hydrogen bonding. As pressure is increased up to 100 GPa, the oxygen-oxygen distance decreases, and the molecular phase VII, where the proton tunnels between a covalent and a hydrogen bond, transforms into the nonmolecular phase X, where the proton lies midway between the oxygens in a symmetric configuration. This structural phase transition, first predicted in 1972 [5], was confirmed by infrared (IR) and Raman experiments to take place at ambient temperature and pressures around $P_t \simeq 65$ GPa [6–10]. These experiments showed that the OH stretching mode softens at the transition, resulting in a cascade of Fermi resonances with the other modes that depend little on pressure [8]. However, the importance of NQE in the transition remains elusive, and the classical Landau picture is recovered only through a phenomenological Hamiltonian where the mode coupling is fitted to the experimental data [8–10].

On the theoretical side, IR absorption spectra computed from Car-Parrinello molecular dynamics simulations at 300 K showed characteristic features at $P_c \simeq 100$ GPa linked to the symmetrization of OH bonds and a marked system anharmonicity at the transition [11]. More recent density functional theory (DFT) calculations, in which the proton is treated

as a classical particle [12,13], systematically overestimate the critical pressure ($\sim$100 GPa) irrespective of temperature. Quantum effects on the nuclei have been studied through *ab initio* path-integral molecular dynamics (PIMD) [14,15], which allowed a step forward in understanding the relevance of NQE in the transition [16–18]. These works showed that the onset of proton delocalization precedes the transition from ice VII to symmetrical ice X and inferred that zero-point motion is responsible for shifting down the transition pressure to 65 GPa. However, because of the purely statistical treatment of proton delocalization in standard PIMD, nothing is known about its dynamical trajectories. As a consequence, not only is a clear-cut definition of the transition pressure difficult in theoretical calculations, but also little connection can be made with experimental vibrational spectra, which, on the contrary, yield a rather precise transition pressure. Moreover, even within a quantum description of the system, a quantitative understanding of the respective contributions of proton tunneling, which is present in phase VII, and of the zero-point energy is still lacking.

In this paper, we report on a study of the ice-VII–ice-X transition based on *ab initio* molecular dynamics with a semiclassical treatment of NQE. In Sec. II, we will present this method, which allows us to treat NQE in the system efficiently, while keeping a fully dynamical description of the system, which means diffusive properties, vibrational spectra, and so on. In Sec. III, our results are then compared to existing PIMD simulations and experimental data in order to validate the use of semiclassical proton dynamics in this problem. Then, in Sec. IV, we will conduct a precise analysis of our results through a one-dimensional phenomenological model. Therefore, we will be able to clearly describe the quantum nature of the transition, even at room temperature.

II. COMPUTATIONAL DETAILS

Computing vibrational spectra through PIMD simulations requires centroid molecular dynamics [19,20] and is therefore

computationally extremely demanding and most often not feasible for systems containing more than a few atoms. Standard PIMD calculations, although less costly, still require a massive computational workload and, on the other hand, only provide statistical properties of the system, leaving out the dynamical aspects of the system. Therefore, as a key to understanding the role of NQE in this transition, we use here a semiclassical method, namely, quantum thermal bath (QTB) molecular dynamics [21,22]. It is based on Langevin dynamics, tailored to reproduce the correct quantum energy distribution through the quantum fluctuation-dissipation theorem [23]. The equation of motion for a degree of freedom x_i with mass m submitted to an external force $f(x_i)$ is then of the usual form:

$$m \frac{d^2 x_i}{dt^2} = f(x_i) - m\gamma \frac{dx_i}{dt} + R(t), \tag{1}$$

where $R(t)$ is a "colored random noise" instead of a Gaussian white noise and γ is a dissipation coefficient. The Fourier transform of the noise $\tilde{R}(\omega)$ and γ are related via the quantum fluctuation-dissipation theorem [23]:

$$|\tilde{R}(\omega)|^2 = 2m\gamma\hbar\omega \left[\frac{1}{2} + \frac{1}{\exp\left(\frac{\hbar\omega}{kT}\right) - 1} \right], \tag{2}$$

where k is the Boltzmann constant. This expression yields the exact quantum energy distribution and vibrational spectra in the system in the case of a harmonic potential [22]. Despite its inherent semiclassical nature, this approach has also been successfully applied in anharmonic systems to study vibrational spectra in molecules [24], Wigner distributions in model systems [25], and methane under shock compression [26]. It was also applied in the study of various other problems, such as isotope effects in crystals [27], mode coupling to the electromagnetic field in nanoparticles [28], and heat capacity of carbon nanotubes and polyethylene [29].

For the present study, we implemented the QTB molecular dynamics into the QUANTUM ESPRESSO package [30]. We performed simulations of a cell containing 54 water molecules,

initially arranged in the ice-VII geometry. The nuclear dynamics is governed by a Langevin equation with coupling to a QTB [22], while the electronic structure is treated by the DFT within the generalized gradient approximation (GGA) approximation [31] to compute the force f in Eq. (1). We checked that the van der Waals contributions to the functional [32] have negligible effects in our high-pressure study. Indeed, discrepancies between the calculated energies and phonon frequencies with or without those terms are much smaller than the error bar due to, for example, the finite length of our trajectories (see the Appendix).

We used ultrasoft pseudopotentials as available in the QUANTUM ESPRESSO code [30]. The electronic wave functions were expanded in plane waves up to a kinetic cutoff of 30 Ry, and the convergence of total energy and forces were accurately checked. Constant-volume simulations were run at room temperature with damping coefficients [γ in Eq. (1)] of 333 or 3.33 cm^{-1} (simulation results differ only in the widths of the spectra); run lengths after equilibration were up to 29 ps long, with an integration time step of 0.484 fs. The lattice parameter was varied from 18 to 14.5 bohrs, thus spanning a pressure range from 12 to 180 GPa. The pressure was computed through the stress theorem [33], and the kinetic contribution is negligible at all volumes considered here.

III. MOLECULAR DYNAMICS RESULTS

A. Static properties of ice

Figure 1 shows the computed OH pair-correlation function at different pressures (left panel). In both Langevin (without NQE) and QTB cases, the low-pressure results consist of two peaks, denoting two different bond lengths: short (~1.1 Å) for covalent OH bonds and long (~1.4 Å) for compressed hydrogen H-O bonds. In the classical Langevin simulation, for $P \leqslant 40$ GPa, the proton never switches between the two bonds as the two peaks are well defined with $g(r) = 0$ between them. When pressure increases, these two peaks merge progressively,
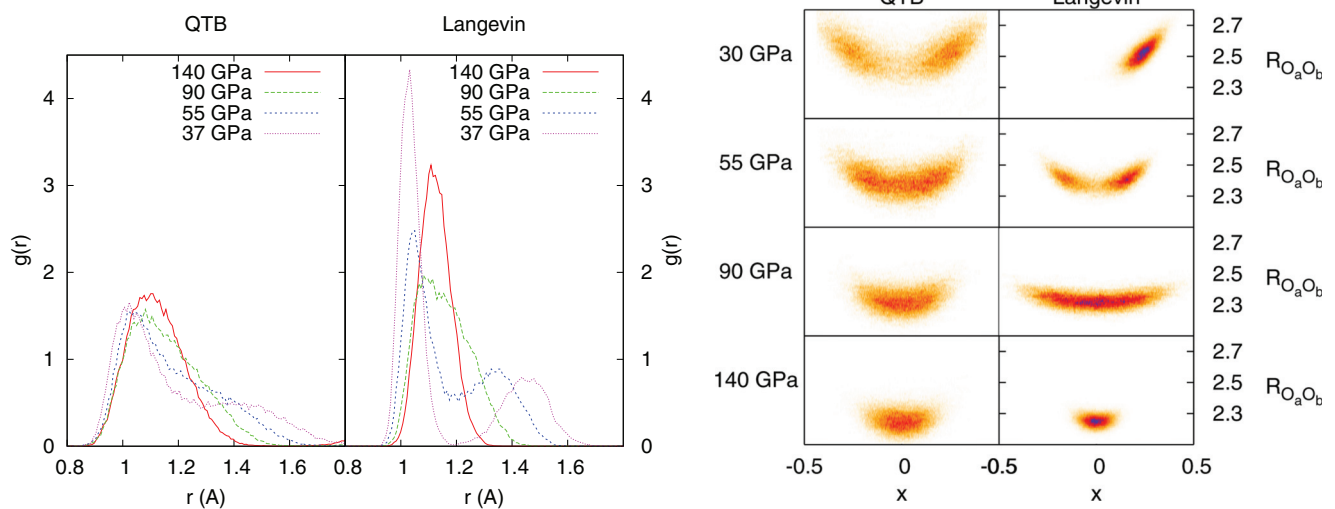

FIG. 1. (Color online) (left) Oxygen-proton pair correlation function $g(r)$ as a function of the OH distance and (right) average proton distribution function $P(x, R_{O_a O_b})$ (with no configurational average; see text) of the proton position x and the OO distance $R_{O_a O_b}$: comparison of QTB and classical Langevin simulations at 300 K.

until the proton is localized in the middle of the bond. In contrast, with QTB the peaks are broader, thus revealing looser bonds, and merge at lower pressure.

For the sake of comparison with PIMD simulations [16–18], we show in Fig. 1 (right panel) the average proton distribution $P(x, R_{O_aO_b})$ as a function of the proton position along the OO segment (x corresponds to $\delta/2$ in Ref. [16]), and the corresponding OO distance $R_{O_aO_b}$. One should note that the distribution function $P(x, R_{O_aO_b})$ is averaged over one trajectory with no configurational averaging. Indeed, in the case of a double-well potential, one needs to average over trajectories with different initial conditions in order to obtain the expected symmetric probability distribution function. Here, we are interested in the probability of the particle crossing the barrier at some point along its trajectory. Therefore, at low pressure, $P \simeq 30$ GPa, the proton is localized on one site in the classical frame, which shows explicitly that it never hops from one well to the other; indeed, thermal fluctuations are not important enough at this pressure to induce a delocalization of the classical proton. In contrast, it is delocalized over two sites with QTB, meaning that during the course of its trajectory, the proton passes from one well to the other. Within QTB, the zero-point energy is thus properly accounted for, and the proton can jump back and forth through the energy barrier for pressures as low as 30 GPa. The increasing pressure lowers the energy barrier between the two minima, thus allowing even the classical proton to hop between the two sites, as revealed by the $P(x, R_{O_aO_b})$ function at 55 GPa in the classical simulation. At 90 and 140 GPa, both methods show a unimodal distribution centered at $x = 0$, corresponding to ice X. The distribution functions provided by QTB simulations are similar to those from *ab initio* PIMD calculations [16], with the onset of proton tunneling occurring at lower pressure in our simulations because of the higher temperature (300 K instead of 90 K in Ref. [16]).

Both the PIMD [16–18] and our QTB results point out that NQE are significant and must be included for an accurate description of the transition. However, in both cases, proton tunneling tends to blur the transition in which the transformation of the two-peak probability distribution into a single peak is continuous.

B. Simulated vibrational spectra

In contrast to the progressive change of OH distribution functions, IR [6–9] and Raman [10] scattering experiments results display a relatively precise transition pressure at approximately 65 GPa. Thus, vibrational properties, which are naturally computed from the semiclassical trajectories, at variance with PIMD, are a clue to identify the transition precisely. The simulated spectra are calculated through the Fourier transform of the nucleus autocorrelation function at different pressures:

$$I(\omega) \propto \sum_l \left| \int r_l(t) e^{i\omega t} \, dt \right|^2, \tag{3}$$

where $r_l(t)$ is the position of the atom l ($l = $ H,O) projected on the OO segment at time t. Figure 2 shows the spectra obtained for different pressures: we can clearly see a broadening and
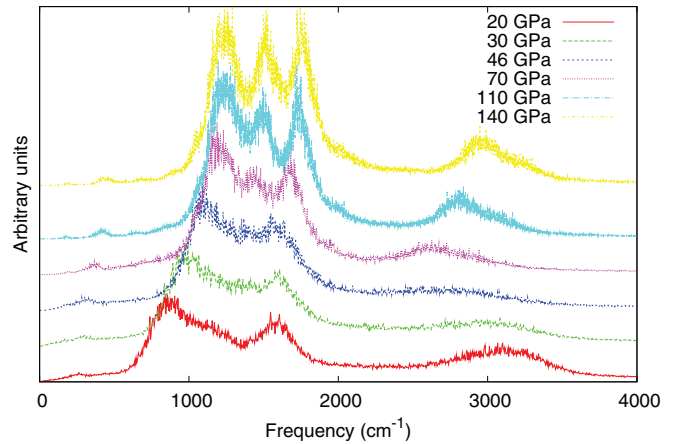

FIG. 2. (Color online) Vibrational spectra in ice obtained via QTB simulations for pressures from 20 to 140 GPa (the spectra have been shifted for clarity).

softening of the high-frequency mode. We then extract the mode frequencies and widths from these spectra.

First, we compare the overall spectra with experimental raw data. As shown in Fig. 3, we obtain excellent agreement with both IR [6–9] and Raman [10] measured frequencies: for $P < 50$ GPa, the modes obtained through QTB simulations can be identified with the experimental spectra, and their symmetries can thus be distinguished. In the 50–100 GPa range, the high-frequency mode displays considerable broadening, which is consistent with the mode couplings shown experimentally. For $P > 100$ GPa, the proton has one equilibrium position even in the classical frame. Therefore, a dynamical matrix analysis
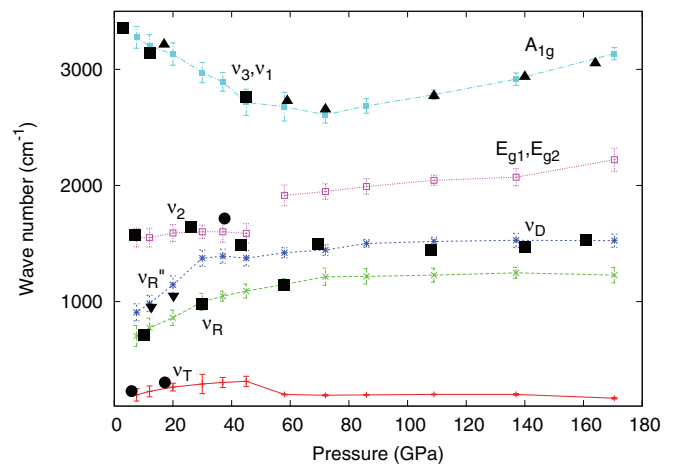

FIG. 3. (Color online) Vibrational frequencies and widths obtained with QTB at ambient temperature up to 180 GPa. Selected infrared (inverted triangles [9] and solid squares [8]) and Raman (solid circles [10]) experimental data: ν_T is the oxygen translational vibration, ν_R and ν_R'' are rotational vibrations of the H_2O molecule, ν_2 is the OH bending vibration, ν_1 and ν_3 are the symmetric and asymmetric OH stretching vibrations, ν_D is the deformational mode, A_{1g} is a symmetric stretching mode, and E_{g1}, E_{g2} are bidimensional vibrations. The solid triangles are the highest LO frequency estimated in Ref. [8]. The softening of the OH stretching mode indicates the transition from phase VII to phase X of ice.

through DFT yields the same modes as those calculated from autocorrelation functions in Eq. (3) and allows the determination of the symmetries of the high-pressure modes. Thus, the asymmetric OH stretching mode ν_3 is responsible for the symmetrization of H bonds in the transition. As pressure approaches 65 GPa, ν_3 undergoes a significant softening and broadening. Here, interactions and coupling between the different vibrations imply this mode never softens to zero as in the standard Landau picture for second-order transitions but presents a clear minimum at the transition.

This spectral analysis is in excellent agreement with the experimental vibrational data [6–10] rendering a transition pressure in the 60–70 GPa range. However, two questions remain open: how do NQE shift the transition pressure down to 60–70 GPa with respect to 100 GPa as predicted for the classical proton [11–13], and how can the progressive character of the proton delocalization [16,17] be reconciled with the singularity of the soft mode in the vibrational spectra [6–10]? In order to get more insight into this subtle matter, we analyze the case of a single proton trapped in a one-dimensional (1D) effective potential and provide below a clear and simple transition scheme.

IV. STUDY OF A PHENOMENOLOGICAL MODEL

One-dimensional models have been used extensively in order to show the existence of three distinct regimes for the proton in ice under pressure [17,18]. Instead, we present here a mapping between our model and the QTB simulations: the proton position x is varied along a fixed OO segment, and for each position, the energy is determined by static DFT calculations, yielding an effective potential $V(x)$. Indeed, because of the cubic structure of phase VII, one OO distance is representative for the whole system. The parameters of $V(x)$

are then fitted so that the exact density matrix calculated via the Schrödinger equation is consistent with the distributions shown in Fig. 1. Such a potential can thus be viewed as a mean-field approximation for the quantum proton around the phase transition. The expression of the potential, inspired from the Landau model of phase transitions, where the role of temperature is replaced by pressure, is written as

$$V(x) = ax^4 + b(P - P_c)x^2 + V_0, \qquad (4)$$

where $a = 12.2 \, \mathrm{eV/\mathring{A}^4}$, $b = 1807.9 \, \mathrm{eV/(\mathring{A}^2\,GPa)}$, and $P_c = 100$ GPa are fitting parameters. As the pressure P increases towards P_c, the two minima at $x_{\mathrm{eq}} = \pm\sqrt{\frac{b}{2a}(P_c - P)}$ move closer to each other, and the barrier height decreases. At the classical transition pressure P_c, the barrier vanishes. The problem thus reduces to a time-independent Schrödinger equation for a proton in one dimension: a finite differences method turns it into an eigenproblem which is easily solved by standard linear algebra procedures.

A. NQE shift the transition pressure

Typical eigenstates are shown in Fig. 4 below the classical transition, at 50 and 80 GPa, and above the classical transition, at 110 GPa: the ground-state wave function undergoes a topological change when its local minimum at $x = 0$ becomes a maximum, between 50 and 80 GPa, with no further modification between 80 and 110 GPa. This phenomenon is the signature of a quantum phase transition undergone by the system [34]. Moreover, in order to quantify the quantum tunneling of the proton, we express the current through the barrier at $x = 0$ as $J(0) = -(\hbar/m)\Psi_1(0)\Psi_2'(0)$ [35], where Ψ_i is the wave function of state i, Ψ_i' is the derivative with respect to x, and E_i is its eigenenergy. The Schrödinger equation then provides a relation between $J(0)$ and the hopping rate Γ_{12}
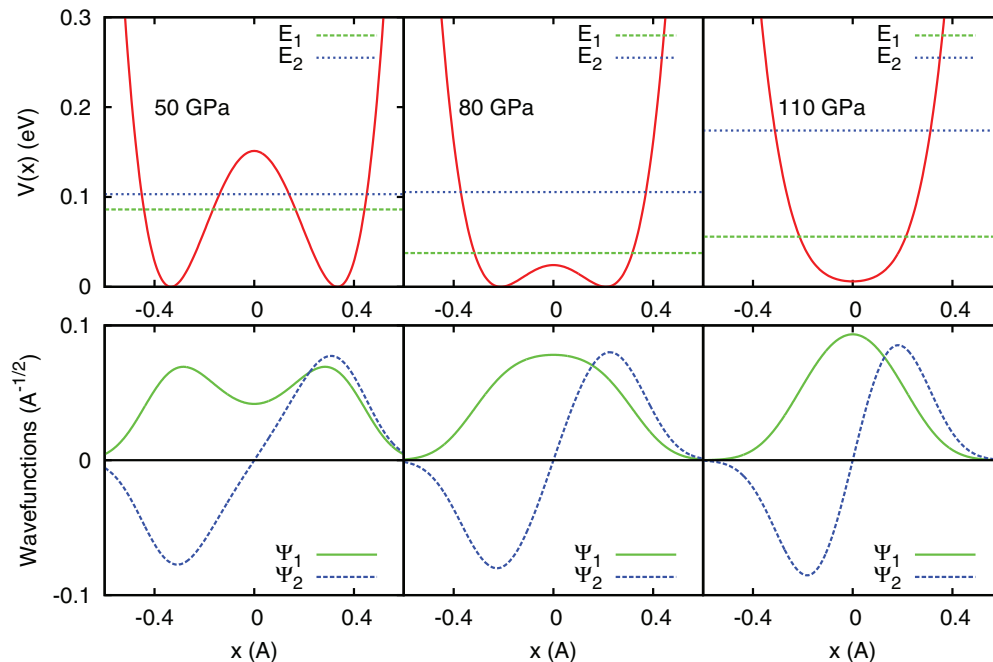

FIG. 4. (Color online) (top) Potential $V(x)$ at 50, 80, and 110 GPa with the ground-state energy E_1 and the energy of the first excited state E_2. (bottom) Wave functions of the ground state, $\Psi_1(x)$, and the first excited state, $\Psi_2(x)$.
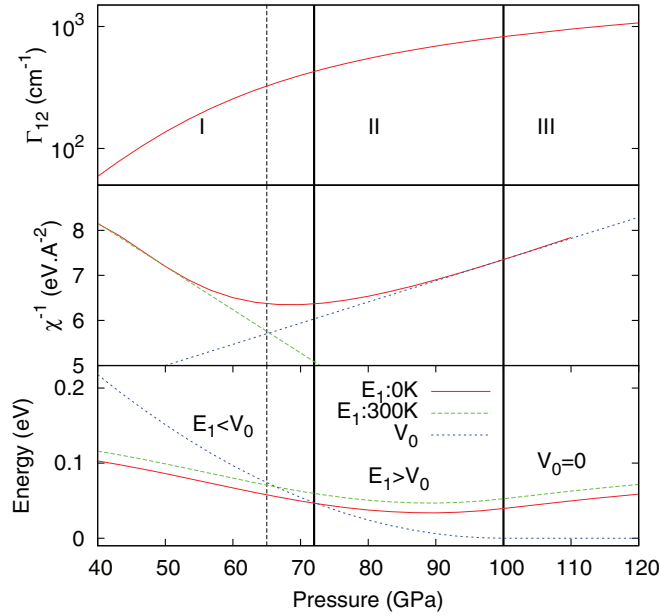
FIG. 5. (Color online) From top to bottom: dependence on pressure of the tunneling rate Γ_{12} (logarithmic scale) in cm^{-1}, the inverse susceptibility χ^{-1} in eV Å^{-2} at 300 K, and the energy barrier V_0 (blue curve) and the ground-state energy E_1 (at $T = 0$ and 300 K) in eV. Three distinct regimes are identified, $E_1 < V_0$ (I), $E_1 > V_0$ (II), and $V_0 = 0$ (III). The transition occurs at the crossing from regime I to regime II, approximately 70 GPa at 0 K, which is then shifted down to 65 GPa at 300 K.

between the two wells [36]:

$$\Gamma_{12} = \frac{E_2 - E_1}{\hbar} = -\frac{\hbar}{2m} \frac{\Psi_1(0)\Psi_2'(0)}{\int_{-\infty}^0 \Psi_1\Psi_2 \, dx}. \qquad (5)$$

Therefore, three regimes are distinguished in Fig. 5:

(I) $P \leqslant P_t$, $E_1 < V_0$ ($V_0 \neq 0$),

(II) $P \geqslant P_t$, $E_1 > V_0$ ($V_0 \neq 0$),

(III) $V_0 = 0$.

In regime I, the onset of tunneling leads to the proton hopping from one well to the other: therefore, Γ_{12} increases rapidly. However, the ground-state energy E_1 remains lower than the barrier, resulting in a wave function with two maxima and a local minimum at $x = 0$.

In regime II, the zero-point energy E_1 is higher than V_0, leading to a maximum of the density at $x = 0$: the proton is mostly localized around the center of the OO distance, even though the barrier has not yet disappeared ($V_0 \neq 0$). Quantum tunneling is responsible for the delocalization of the proton over the two potential wells in regime I, but the transition occurs when the zero-point energy reaches the barrier height. The increase in Γ_{12} is slowed down because tunneling does not occur anymore in regime II.

In regime III, the barrier has disappeared ($V_0 = 0$), and the proton confinement is only due to contraction of the OO distance.

Therefore, the quantum phase transition occurs when the zero-point energy reaches the height of the barrier at approximately 70 GPa, at which point the ground-state wave function shows a change in nature.

B. Thermal fluctuation contribution

The previous analysis, which was done at $T = 0$ K, can be extended to finite temperatures through simple arguments. The thermal energy associated with a temperature of 300 K is about 26 meV, which is half the barrier height at the transition for $T = 0$ K (about 54 meV). Thus, taking into account the thermal fluctuations leads, to a first approximation, to an upward shift of the energy (see bottom of Fig. 5). The transition pressure, determined by the point where the energy is equal to the barrier height, is therefore reduced from 70 to approximately 65 GPa. First, this is in excellent agreement with the value found via IR and Raman measurements [6–10] and independently with our QTB simulations. Second, even at high temperatures, the contribution from quantum zero-point motion is far from negligible, inducing a massive change in the value of the transition pressure (a decrease of about 40%), and is even dominant compared to the effect of thermal fluctuations (about 5%). This shows the possibility of having quantum-driven phase transition in a real system at room temperature and reinforces the importance of correctly treating NQE.

C. Proton delocalization and soft mode

In order to show the connection between the topological change in the ground state and the mode softening, we compute the quantum susceptibility from linear response theory [37]. Kubo's formalism gives an explicit expression for the susceptibility in terms of the system's eigenstates, which we computed for the one-dimensional system:

$$\chi = \int_0^\beta d\lambda \, \langle \hat{x}(-i\hbar\lambda)\hat{x} \rangle - \beta \langle \hat{x}^0 \hat{x}^0 \rangle, \qquad (6)$$

where $\beta = (k_B T)^{-1}$ and $\hat{x}^0$ is the diagonal part of the position operator $\hat{x}$ ($\langle \cdot \rangle$ indicates the expectation value at equilibrium). This expression contains both the quantum and the thermal contributions to the fluctuations of the system. At 300 K, well below the transition, Ψ_1 and Ψ_2 are degenerate, and the first relevant excited state is Ψ_3; above the transition, the degeneracy between states 1 and 2 is lifted, and the first relevant excited state is Ψ_2.

Figure 5 shows the evolution of the inverse susceptibility with pressure. In the classical picture, χ^{-1} is proportional to the square of the soft-mode frequency; quantum fluctuations of the proton position are maximum at the transition, which implies a minimum of χ^{-1}. In both the classical and the quantum cases, χ^{-1} is linear with P well below and above the transition, but the transition pressure $P_t \simeq 65$ GPa is lower than its classical counterpart, displaying the same behavior as ν_3, the OH stretching mode in ice (Fig. 3). Hence, the increase in proton tunneling and delocalization translates into an increase of its fluctuations which corresponds to a decrease of the frequency of its associated vibration mode. After the transition, the contraction of the potential leads to a gradual confinement of the proton, diminishing its fluctuations, which implies an increase of the frequency of its vibrations. This formalism also validates our first approximation of the thermal energy contribution to the transition pressure.

TABLE I. Relative difference of the energy of the system $\Delta E / E$ obtained with or without van der Waals contributions to the functional after relaxation of a cell containing 54 water molecules for different pressures.

Pressure (GPa)	Relative difference of energy $\Delta E / E$
7	0.00058
20	0.00072
32	0.00073
49	0.00079
71	0.00079
108	0.00078

V. CONCLUSION

To conclude, we performed *ab initio* simulations on high-pressure ice including the QTB method for a semiclassical description of NQE, which allowed a very efficient and computationally undemanding treatment of the quantum nature of protons. Consistent with PIMD calculations, our results showed the onset of proton tunneling at pressures as low as 30 GPa, well below the classical transition pressure $P_c = 100$ GPa [11–13]. On the other hand, we provide results with respect to full-fledged PIMD methods: our approach yields semiclassical proton trajectories from which we calculated the vibrational spectra, which are in excellent agreement with IR [6–9] and Raman [10] measurements.

Therefore, the transition from ice VII to ice X was seen through two different aspects: the continuous modification of the proton distribution functions, where two peaks merge at the transition, and the softening of the OH stretching mode which indicates a clear transition pressure of $P_t \simeq 65$ GPa. The QTB simulations then allowed for a simple mapping to an effective 1D model, for which the exact quantum solution of the Schrödinger equation can be computed. First, at $T = 0$ K, a true quantum phase transition occurs when the ground-state energy reaches the barrier height, well before the barrier disappears. This leads to an exact and theoretically rigorous definition of the transition pressure. Then, thermal effects can be included: to a first approximation, the energy is just shifted by $k_B T$, but an exact treatment of both quantum and thermal fluctuations is achieved through the quantum susceptibility. The final calculations show that quantum zero-point energy motion is much more important than thermal fluctuations, even at 300 K. This formalism also provides the direct connection between the proton delocalization and the soft mode in the spectra.

Hence, the combination of spectral analysis and 1D mapping leads to a well-rounded and fully consistent description of
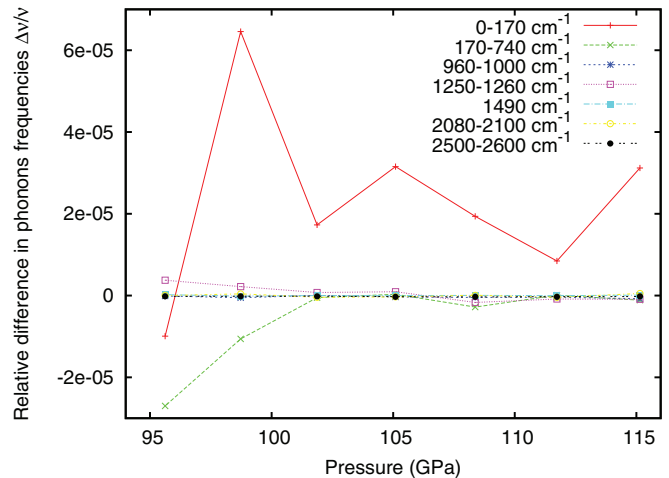

FIG. 6. (Color online) Relative difference of phonon frequencies $\Delta \nu / \nu$ calculated with or without van der Waals contributions to the functional for each phonon in the high-pressure system.

a textbook quantum-driven phase transition, while at the same time showing that semiclassical approaches for NQE are very efficient and accurate and might thus have a potentially large impact on the broad community studying real, large systems at room temperature.

APPENDIX: DETAILS ON THE VAN DER WAALS CONTRIBUTIONS TO THE FUNCTIONAL

In order to determine the effects of van der Waals contributions to the functional in our calculations, we performed simulations on a cell containing 54 water molecules and compared the energies obtained after relaxation (Table I), as well as phonon frequencies (Fig. 6), to the results obtained without van der Waals contributions.

The relative difference of the energy in the system is approximately 10^{-3} (Table I), while the relative difference in the phonon frequencies (Fig. 6) is about 10^{-5} for high-frequency modes and 10^{-4} for low-frequency modes. Therefore, the effects of the van der Waals contributions to the functional are negligible in our high-pressure study.

[1] T. Miyazaki, in *Atom Tunneling Phenomena in Physics, Chemistry and Biology* (Springer, Berlin, 2004), p. 263.

[2] K. D. Kreuer, S. J. Paddison, E. Spohr, and M. Schuster, Chem. Rev. **104**, 4637 (2004).

[3] H. S. Lee and M. E. Tuckerman, J. Phys. Chem. C **112**, 9917 (2008).

[4] L. Buannic, F. Blanc, D. S. Middlemiss, and C. P. Grey, J. Am. Chem. Soc. **134**, 14483 (2012).

[5] W. B. Holzapfel, J. Chem. Phys. **56**, 712 (1972).

[6] A. F. Goncharov, V. V. Struzhkin, M. S. Somayazulu, R. J. Hemley, and H. K. Mao, Science **273**, 218 (1996).

[7] K. Aoki, H. Yamawaki, and M. Sakashita, Phys. Rev. Lett. **76**, 784 (1996); K. Aoki, H. Yamawaki, M. Sakashita, and H. Fujihisa, Phys. Rev. B **54**, 15673 (1996).

[8] V. V. Struzhkin, A. F. Goncharov, R. J. Hemley, and H. K. Mao, Phys. Rev. Lett. **78**, 4446 (1997).

[9] M. Song, H. Yamawaki, H. Fujihisa, M. Sakashita, and K. Aoki, Phys. Rev. B **60**, 12644 (1999).

[10] A. F. Goncharov, V. V. Struzhkin, H. K. Mao, and R. J. Hemley, Phys. Rev. Lett. **83**, 1998 (1999).

[11] M. Bernasconi, P. L. Silvestrelli, and M. Parrinello, Phys. Rev. Lett. **81**, 1235 (1998).

[12] X. Z. Lu, Y. Zhang, P. Zhao, and S. J. Fang, J. Phys. Chem. B **115**, 71 (2011).

[13] L. Tian, A. I. Kolesnikov, and J. Li, J. Chem. Phys. **137**, 204507 (2012).

[14] B. J. Berne and D. Thirumalai, Annu. Rev. Phys. Chem. **37**, 401 (1986).

[15] D. Marx and M. Parrinello, J. Chem. Phys. **104**, 4077 (1996).

[16] M. Benoit, D. Marx, and M. Parrinello, Nature (London) **392**, 258 (1998).

[17] J. A. Morrone, L. Lin, and R. Car, J. Chem. Phys. **130**, 204511 (2009).

[18] L. Lin, Ph.D. thesis, Princeton University, 2011, https://web.math.princeton.edu/~linlin/Thesis_LinLin.pdf.

[19] J. Cao and G. A. Voth, J. Chem. Phys. **100**, 5093 (1994); **100**, 5106 (1994); **101**, 6157 (1994); **101**, 6168 (1994).

[20] A. Witt, S. D. Ivanov, M. Shiga, H. Forbert, and D. Marx, J. Chem. Phys. **130**, 194510 (2009).

[21] M. Ceriotti, G. Bussi, and M. Parrinello, Phys. Rev. Lett. **103**, 030603 (2009).

[22] H. Dammak, Y. Chalopin, M. Laroche, M. Hayoun, and J. J. Greffet, Phys. Rev. Lett. **103**, 190601 (2009).

[23] H. B. Callen and T. A. Welton, Phys. Rev. **83**, 34 (1951).

[24] F. Calvo, N. T. Van-Oanh, P. Parneix, and C. Falvo, Phys. Chem. Chem. Phys. **14**, 10503 (2012).

[25] M. Basire, D. Borgis, and R. Vuilleumier, Phys. Chem. Chem. Phys. **15**, 12591 (2013).

[26] T. T. Qi and E. J. Reed, J. Phys. Chem. A **116**, 10451 (2012).

[27] H. Dammak, E. Antoshchenkova, M. Hayoun, and F. Finocchi, J. Phys. Condens. Matter **24**, 435402 (2012).

[28] Y. Chalopin, H. Dammak, M. Laroche, M. Hayoun, and J. J. Greffet, Phys. Rev. B **84**, 224301 (2011).

[29] S. Buyukdagli, A. V. Savin, and B. B. Hu, Phys. Rev. E **78**, 066702 (2008).

[30] P. Giannozzi *et al.*, J. Phys. Condens. Matter **21**, 395502 (2009).

[31] J. P. Perdew, K. Burke, and M. Ernzerhof, Phys. Rev. Lett. **77**, 3865 (1996).

[32] S. Grimme, J. Antony, S. Ehrlich, and H. Krieg, J. Chem. Phys. **132**, 154104 (2010).

[33] O. H. Nielsen and R. M. Martin, Phys. Rev. B **32**, 3792 (1985).

[34] D. Schwandt, F. Alet, and S. Capponi, Phys. Rev. Lett. **103**, 170501 (2009).

[35] Y. Dakhnovskii, B. Bursulaya, and H. J. Kim, J. Chem. Phys. **102**, 7838 (1995).

[36] A. Messiah, in *Quantum Mechanics* (Dover, New York, 1958), Chap. IV, p. 121.

[37] R. Kubo, Rep. Prog. Phys. **29**, 255 (1966).